Tropical Rainfall Variability on Interannual-to-Interdecadal/Longer-Time Scales Derived from the GPCP Monthly Product

Guojun Gu[#], Robert F. Adler[@], George J. Huffman[&], and Scott Curtis[+]*

[#] Goddard Earth Sciences and Technology Center, University of Maryland Baltimore County, Baltimore, MD, and Laboratory for Atmospheres, NASA Goddard Space Flight Center, Greenbelt, MD

[@] Laboratory for Atmospheres NASA Goddard Space Flight Center, Greenbelt, MD

[&] Science Systems and Applications Inc, and Laboratory for Atmospheres, NASA/Goddard Space Flight Center, Greenbelt, MD

[+] Department of Geography, East Carolina University, Greenville, NC

Journal of Climate

* Corresponding author address: Guojun Gu, Code 613.1, NASA/GSFC, Greenbelt, MD 20771.

ggu@agnes.gsfc.nasa.gov

Abstract

Global and large regional rainfall variations and possible long-term changes are examined using the 26-year (1979-2004) GPCP monthly dataset (Adler *et al.,* 2003). Our emphasis is to discriminate among variations due to ENSO, volcanic events, and possible long-term climate changes in the tropics. Although the global linear change of precipitation in the data set is near zero during the time period, an increase in tropical rainfall is noted, with a weaker decrease over northern hemisphere middle latitudes. Focusing on the tropics (25°S-25°N), the data set indicates an upward trend (0.06 *mm day^{-1}/decade*) and a downward trend (-0.02 *mm day^{-1}/decade*) over tropical ocean and land, respectively. This corresponds to an about 4.9% increase (ocean) and 1.6% decrease (land) during the entire 26-year time period. Techniques are applied to isolate and quantify variations due to ENSO and two major volcanic eruptions (El Chichón, March 1982; Pinatubo, June 1991) in order to examine longer time-scale changes. The ENSO events generally do not impact the tropical total rainfall, but, of course, induce significant anomalies with opposite signs over tropical land and ocean. The impact of the two volcanic eruptions is estimated to be about a 5% reduction in tropical rainfall over both land and ocean. A modified data set (with ENSO and volcano effects removed) retains the same approximate linear change slopes, but with reduced variance, thereby increasing the confidence levels associated with the long-term rainfall changes in the tropics

1. Introduction

Exploring global climate variability and change has an immense environmental and societal significance (*e.g.,* Kumar *et al.* 2004). Previous studies showed evident interannual variability and interdecadal/longer-term changes in various climate components, *e.g.,* surface air temperature, sea surface temperature (SST), land rainfall, *etc.,* specifically during recent decades (*e.g.,* Cane *et al.* 1997; Chen *et al.* 2002; Simmons *et al.* 2004). The El Niño-Southern Oscillation (ENSO) generally dominates the global variability on interannual time scale (*e.g.,* Trenberth *et al.* 1998; Wigley 2000; Trenberth *et al.* 2002). Other mechanisms such as the Pacific Decadal Oscillation (PDO) and the Arctic Oscillation (AO) are found to be accountable for most of the interdecadal variability (*e.g.,* Zhang *et al.* 1997; Hurrell *et al.* 2001).

Longer-term change and/or trend are also widely recognized, and considered to be a consequence of probably both natural and human-induced effects (*e.g.,* Chu and Wang 1997; Bates and Jackson 2001). The gradually warming climate is a good example (*e.g.,* Yang *et al.* 2003; Neelin *et al.* 2003; Kumar *et al.* 2004). However, whether there is a coherent long-term variation within the entire hydrological cycle accompanying this seemingly expected warm-up is still an outstanding question (*e.g.,* Chen *et al.* 2002; Simmons *et al.* 2004; McCarthy and Toumi 2004; Yin *et al.* 2004). This is mostly due to the lack of long-record, consistent observations of fundamental climate components, particularly precipitation over the globe. With the availability of the 26-year (1979-2004) monthly rainfall product from the Global Precipitation Climatology Project (GPCP) (Adler *et al.,* 2003), it is thus worthwhile to examine global rainfall variability on both interannual and interdecadal/longer-term time scales. With the relatively short 26-year record firm conclusions to long-term changes may be difficult, but an improved understanding of general mechanisms controlling the response of the global hydrological cycle may be possible.

The purpose of this study is therefore to make efforts along this direction, specifically to discriminate among the rainfall variations due to ENSO, volcanic events, and possible long-term changes, particularly in the tropics.

2. Brief Description of Data

The monthly precipitation dataset from the Global Precipitation Climatology Project (GPCP) is a community-based analysis of global precipitation under the auspices of the World Climate Research Program (WCRP) from 1979 to the present. On a global $2.5°\times2.5°$ grid, the data is combined from various information sources: microwave-based estimates from Special Sensor Microwave/Imager (SSM/I), infrared (IR) rainfall estimates from geostationary and polar-orbiting satellites, and surface rain gauges. The analysis procedure is designed to take advantage of particular strengths of the individual input data sets, especially in terms of bias reduction. For example, the microwave information over the ocean is used to adjust the bias of the IR-based estimates and the gauge information is used to adjust the bias of the merged satellite estimates over land. The data set therefore should have the low bias of the input information deemed to be best, with the superior sampling on a monthly scale produced by multiple satellites. The period from 1988 to the present is homogeneous in terms of input data sets; however, to extend the data set back to 1979 the developers are limited to using infrared-based estimates with regard to satellite observations. Although these pre-1988 estimates are trained on the later period to reduce possible differences, there is still a time inhomogeneity in the analysis, in terms of satellite input data sets. These features of the data set are considered in the following analysis. Further information about the GPCP monthly dataset is detailed in Adler *et al.* (2003) and Huffman *et al.* (1997).

4

3. Results

Tables 1-3 provide a summary of the mean rain rates around the globe, and their standard deviations from corresponding mean seasonal cycles. Various latitudinal belts over both land and ocean are applied to give a global and large regional description of mean precipitation and variability. Larger variability (>10%) is generally seen in the mid-high latitudes except over land along the latitude band of 50°S-90°S. Interestingly, the variabilities in the global total are much weaker than these within various latitude bands, tending to suggest a conservation of precipitation, with opposite rainfall anomalies at different regions across the globe at longer-than-season time scales, particularly on the interannual time scale.

The 26-year time history of the data indicates no significant linear trend in the annual global mean precipitation (solid line in Fig. 1), resulting from possible weak, opposite trends over land and ocean (Fig. 1). An upward (downward) linear trend is found in the oceanic (land) mean precipitation. Evidence of regional trends is also apparent. Fig. 2 shows a description of rainfall changes by ocean/land and latitude band contributions to the global total change. It is evident that the large changes are in the tropics and northern hemisphere mid-latitudes. Zonally-averaged GPCP data combining land and ocean indicate the possibility of generally increasing precipitation (about 3% over 26 years) in deep tropics (25°S-25°N), with the increase focused on the ocean (4.9% increase), and a smaller (1.6%) decrease over land. In the northern subtropics (25°N-50°N) a decrease over land and ocean is noted in the data set.

Since space-borne microwave observations of precipitation became available only after 1987, linear changes are further estimated during the 1988-2004 period for comparison (Fig. 3). As during 1979-2004, tropical rainfall variability, particularly over tropical oceans, dominates.

5

The changes for this shorter period are similar to the longer period in the tropics, although the small change over tropical land alters sign. We also note that there is a much more intense change in the global total precipitation primarily due to a much weaker rainfall change along 25°N-50°N during this time period. Certainly, these results warrant at least a careful analysis of the confidence limits we can determine for these statistics. Also, possible mechanisms have yet to be further explored, though the changes of the Hadley circulation strength might be an interpretation (*e.g.,* Chen *et al.* 2002).

In the next three subsections, we will thus focus on the tropics (25°S-25°N) because of the most intense long-term rainfall changes occurring in this region (Figs. 2, 3) and the greater confidence of the authors in the quality of the precipitation analysis in the tropics, in terms of detecting small, longer-term rainfall signals. The impact of ENSO and volcanoes will be first investigated to isolate, as much as possible, their effects on surface rainfall. We then re-examine the long-term rainfall variability with and without the ENSO and volcanic impact. Also, to limit high-frequency noises, annual mean rainfall anomalies will be the primary variable examined for long-term changes.

3.1 ENSO and volcanic impact

The time series of tropical monthly mean rainfall anomalies are depicted in Fig. 4a, similar to Fig. 8 in Adler *et al.* (2003). The ENSO impact is evident (Fig. 4b). Generally, the warm (cold) events correspond to more (less) rainfall over ocean (land). Strong variabilities can be seen in tropical total rainfall, but are weaker than rainfall variations over land and ocean, separately. This is due to the opposite effects of ENSO on rainfall over land and ocean (*e.g.,* Neelin *et al.* 2003).

6

Two major volcanic events occurred during the data record. The El Chichón volcano erupted in March 1982, and Pinatubo in June 1991. Following these two large eruptions, abrupt changes showed up in the global mean stratospheric aerosol optical thickness (τ_{st}) due to the injection of aerosol particles (Fig. 4c) (Sato *et al.* 1993). These changes tend to effectively influence the radiation budget of Earth (*e.g.*, Robock 2000). Past studies discovered that volcanic eruption could cause significant global cooling and drying, and also impact precipitation efficiency through radiative forcing and aerosol particles injected into the atmosphere (*e.g.*, Spencer *et al.* 1998; Robock 2000; Soden *et al.* 2002; Yang and Schlesinger 2002). Also, the impact may last at least 1-2 years (*e.g.*, Robock 2000; Yang and Schlesinger 2002).

Volcanic impact is discernible in the tropical rainfall anomalies (Fig. 4a), though it is compounded with the influence of ENSO. To emphasize volcanic impact, annual mean rainfall anomalies[1] over ocean (P_O) versus land (P_L) are plotted in Fig. 5. Volcano years are identified by choosing a threshold of τ_{st}, *i.e.*, at least six months with $\tau_{st} \geq 0.02$ for each year (horizontal dotted line in Fig. 4c), yielding six volcano years, *i.e.*, 1982, 1983, 1984, 1991, 1992, and 1993. A linear regression relation is further estimated between P_O and P_L during the normal (non-volcano) years (dashed line in Fig. 5). As expected, P_O always tends to be opposite of P_L, and they both generally approach the regression line very well except in 1983 and 1991 in which the volcanic impact is strong. This is the major reason for a much weaker year-to-year fluctuation in the tropical total precipitation (solid lines in Figs. 4a, 9a), compared to ocean or land values alone. Volcanic signals can also be seen in 1992, though relatively weaker. Quantitatively these two eruptions may have induced up to a 5% rainfall decrease in the tropics during 1983 and

---

[1] The time series of annual mean rainfall anomalies are de-trended as we focus on the interannual-to-interdecadal variability first.

7

1991. The effect is evident over both land and ocean. In the other three volcano years defined by τ_{st}, *i.e.*, 1982, 1984, 1993, P_O and P_L tend to approach the regression line as in most normal years, probably suggesting that the rainfall anomalies were more sensitive to the lower boundary forcing for some reasons, such as a comparatively strong SST forcing at the earlier stage of volcanic eruption (1982), and/or the completing of atmospheric vertical adjustment to aerosol forcing at the later stage of volcanic eruption (1984, 1993). However, detailed mechanisms have yet to be investigated.

We now focus on assessing the impact of ENSO and volcanoes using the time series of monthly rainfall anomalies. Again, these time series are first de-trended for this particular analysis as we assume that their impact be on the interannual or interdecadal time scale. Interestingly the two volcanic eruptions coincidently occurred with El Niño events (Figs. 4b, 4c). We thus have to discriminate their impact during this period. The whole months during 1979–2004 are first categorized into two time periods: the normal (τ_{st}<0.02) and volcanic impact (τ_{st}≥0.02) months (Fig. 4c). Our strategy is to first estimate the possible relations between rainfall anomalies and ENSO during the normal period, then apply them to the volcano period to isolate the impact of ENSO, and finally estimate the relations between rainfall anomalies and τ_{st} after the ENSO impact is removed from the rainfall anomalies during the volcano period. Because ENSO has opposite effects on rainfall anomalies over land and ocean (Fig. 5), we assume that the ENSO signals are reasonably weak in the tropical total rainfall anomalies (Figs. 4a, 9a). This is consistent with Su and Neelin (2003), who showed that the tropical total precipitation is not a simple, linear response to tropical SST (or ENSO) as tropospheric temperature, but controlled by other factors. Obviously, the success of our strategy heavily depends on whether the impacts of ENSO and volcano are separable given their likely nonlinear

relations (*e.g.,* Wigley 2000).

The rainfall anomalies over ocean, land, and the entire tropics are plotted as function of the ENSO index (Nino3.4) during these two periods (Fig. 6). Over ocean (Fig. 6a), a linear relation is seen between rainfall and Nino3.4 with a slope of 0.0528 *mm day^{-1} per degree* during the normal (non-volcano) period, though there is a large scatter. This relation confirms that tropical oceanic rainfall responds to the SST anomalies associated with ENSO. In contrast, during the volcano period, no significant response of rainfall shows up, probably resulting from the opposite impacts of the El Niño and volcano as they occurred almost simultaneously (Figs. 4b, 4c). Over land (Fig. 6b), rainfall anomalies decrease with the increase of Nino3.4 during both the normal and volcano periods, with the linear slopes of same order: -0.137 and -0.1446 *mm day^{-1} per degree*, respectively. The similar rainfall changes during these two periods indicate that both ENSO and volcano tend to suppress surface rainfall over land. For tropical total precipitation (Fig. 6c), there is a near-zero rainfall change with Nino3.4 (0.0013 *mm day^{-1} per degree*) during the normal period; however, a significant downward slope (-0.0387 *mm day^{-1} per degree*) can be seen during the volcano period. The results confirm that the tropical total precipitation does not systematically respond to the ENSO forcing as mentioned above, but indicate that volcanic eruptions significantly reduce surface rainfall in the entire tropics.

To further focus on the volcanic impact on rainfall changes, the tropical rainfall anomalies during the volcano period are plotted as function of τ_{st} (Fig. 7a). The most intense response is over land due to the same-sign impact of both the warm ENSO and volcano (dashed line). For the tropical total precipitation, an evident negative slope can be seen (solid line). As shown in Fig. 6a, a very weak rainfall response occurs over ocean caused by the opposite effects of the El Niño and volcano. A further assumption is made that the ENSO events consistently

9

impact the rainfall changes during both the normal and volcano periods.

The linear regression relations of the rainfall anomalies versus Nino3.4 over ocean (0.0528 *mm day^{-1} per degree*) and land (-0.137 *mm day^{-1} per degree*) (Figs. 6a, b), respectively, estimated earlier for the normal (non-volcano) period, are then applied to estimate the rainfall response to the warm ENSO during the volcano occurrence. After the ENSO impact is removed in this way, the relationships between rainfall anomalies and τ_{st} are depicted in Fig. 7b. Though still very scattered, the linear fits for rainfall changes over ocean (-1.0594), land (-1.6813), and the entire tropics (-1.2097) are similar. This supports the idea that volcanic eruptions simultaneously reduce rainfall over both land and ocean in the tropics.

3.2 Interannual-to-interdecadal rainfall variability in the tropics

Interannual variability in the monthly rainfall anomalies (Fig. 4a) is further examined with and without the impact of ENSO and volcanoes. We intend to isolate the ENSO signals. A 2-7-year band-pass-filter is applied to isolate the oscillation within this period band. Past studies showed the strong existence of the ENSO signals within this period band. Evident variability appears in the rainfall anomalies over land, and ocean (Fig. 8a). The ENSO events generally force opposite anomalies over land and ocean as discussed above, except near the two volcanic eruptions, resulting in smaller total rainfall anomalies (solid line in Fig. 8a). Particularly during 1994-2004, the variability is negligible compared to strong variations over land and ocean separately. The two volcanic eruptions forced a similar negative tendency of rainfall change over land and ocean, although the reduction of rainfall during 1991 seems to begin prior to the eruption, indicating other possible factors.

The linear regressions of rainfall anomalies with Nino3.4 and τ_{st} obtained in the

preceding section (Figs. 6, 7) are applied to estimate the rainfall responses due to these factors. They are further subtracted from the monthly time series and the anomalies with the period of 2-7-year are estimated (Figs. 8b, 8c). The interannual variability of rainfall anomalies over land and ocean is shown in Fig. 8b without the ENSO impact but with the volcanic impact remaining. Both over ocean and land curves approach the tropical total rainfall oscillation (solid line in Figs. 8a, 8b), although it seems that partial ENSO signals may still be included, particularly after 1994. This is likely because of the simple linear regression relations used here are not completely consistent during the entire period, especially for the strongest ENSO event of the period during 1997-2001. The ENSO events may themselves undergo long-time oscillations (*e.g.,* Vimont *et al.* 2003; Sun *et al.* 2004). Also, the volcanic impact shows a consistent impact on these three time series (Figs. 8b, 8c). Interestingly, even after the impacts of ENSO and volcano are removed, interannual oscillations can still be seen, particularly in the tropical total rainfall. This tends to agree with Su and Neelin (2003).

We then further clarify the ENSO and volcano signals in tropical rainfall anomalies, and demonstrate the success/effectiveness of the method used here by applying spectrum analyses to the various time series with/without the impact of ENSO and volcano (Fig. 9). Three power peaks appear in the tropical oceanic rainfall anomalies at the periods of 2-3, 5, 8-10 years. Similar spectrum features can also be seen in the rainfall anomalies over land with a much stronger peak at the 5-year period (not shown). For tropical total rainfall anomalies, the power peak at the period of 5 years disappears, further confirming the weak impact of ENSO. The existence of oscillations in tropical oceanic rainfall within the period of 2-7 years is consistent with previous studies focusing on SST and surface winds in the equatorial Pacific (*e.g.,* Rasmusson and Carpenter 1982). Within the period of 7-11 years, the spectral signals might not

11

be only ascribed to the ENSO-type interdecadal changes (*e.g.,* Zhang *et al.* 1997; Vimont *et al.* 2003), but probably be contributed by the volcanic eruptions as they appear in both oceanic and total rainfall (solid and dashed lines in Fig. 9).

Spectral analyses are also applied to the time series of tropical oceanic and total rainfall anomalies without the ENSO or volcano signals. The oscillation signals around the 5-year period are greatly suppressed for the oceanic rainfall, partly suggesting the success of the regression method we used. The signals around two other peaks that also appear in the tropical total rainfall are suppressed too, but still very evident. Thus, it seems that other than ENSO, the signals at the 2-3-year period may be related to the tropospheric biennial oscillation (TBO) (*e.g.,* Meehl 1997). On the other hand, within the 7-11-year period band, the appearance of the peak, though becoming much weaker, tends to suggest that the volcanic signals still exist to a certain degree in the time series, implying the difficulties of eliminating their impact.

3.3 Long-term rainfall change

After the impacts of ENSO and volcanoes are isolated, we come back to examine the long-term rainfall change in the tropics. Fig. 10a depicts the time series of annual mean rainfall anomalies over ocean (P_O), land (P_L), and the entire tropics (P_{LO}). Large variations occur in P_L and P_O, and they are mostly opposite. Compared to them, P_{LO} shows much weaker interannual variability as shown in last subsection. Long-term rainfall changes represented by the slopes of regression lines are computed for P_{LO}, P_O, and P_L, respectively. They are the same as in Fig. 2 but denoted by different units (Fig. 10a).

The confidence levels of these changes are further estimated based on the Student's t-test (*e.g.,* Woodward and Gray 1993). The degrees of freedom (*dof*) are estimated by means of

12

$dof=n(1-\gamma)/(1+\gamma)-2$ (*e.g.,* Livezey and Chen 1983; Chu and Wang 1997; Bretherton *et al.* 1999), here n and γ are the length of and the lag-one correlation coefficient for each time series, respectively. For P_O, the linear trend (0.0584 *mm day⁻¹/decade*) is at the 5% level (Table 4), showing a relatively strong upward rainfall increase; a negative trend is seen over land (-0.0192 *mm day⁻¹/decade*), but is not statistically significant; tropical total rainfall shows an upward trend (0.0373 *mm day⁻¹/decade*) at the 10% level. The relatively low confidence levels may partly be related to the length of data record. If time-persistence is assumed for any variability on the interannual-to-interdecadal time scales, roughly 43-year and 51-year data records would be needed for the tropical oceanic and total rainfall to reach the 1% confidence level, respectively.

We again apply the linear relations of monthly rainfall anomalies with the ENSO and volcano effects to remove/limit their signals in the annual mean rainfall anomalies. Our purpose is to examine how the ENSO and volcano signals may influence the statistical confidence level given their strong existence in the annual mean rainfall anomalies (Fig. 10a).

After the impact of ENSO and volcano is limited/removed in the monthly time series, the annual mean time series are reconstructed (Fig. 10b). It is clear that the interannual variability is reduced. As expected, the linear change becomes smaller for P_{LO} because of negative anomalies associated with volcanoes in the earlier time period (Fig. 5). However, the confidence level for the combined ocean/land signal increases from 10% to 4% (Table 4) because of an increased *dof* and reduced variance. Over land, still no significant long-term linear change can be obtained, though the magnitude of the slope increases. The confidence level for tropical oceanic rainfall becomes 1%, in spite of a slightly smaller trend, again due to a larger *dof* and reduced variance. Thus, an upward trend in the tropical oceanic rainfall may exist that is dominant in the tropical total rainfall change.

4. Summary and concluding remarks

Global and large regional rainfall variabilities are examined using the 26-year (1979-2004) GPCP monthly dataset. Attempts have been made to discriminate among the variations resulting from ENSO, volcanoes, and possible long-term climate changes.

ENSO and two major volcanic eruptions during the data record heavily modulate tropical rainfall variabilities. ENSO has opposite effects over land and ocean, with only a negligible influence on the tropical total rainfall. The warm (cold) events tend to increase (decrease) oceanic rainfall, but decrease (increase) rainfall over land. Thus, ENSO is not a major contributor to the interannual variability in tropical total rainfall, though it can cause intense rainfall anomaly features by shifting the major rainy zones in the tropics (*e.g.*, Wigley 2000; Curtis and Adler 2003; Neelin *et al.* 2003). The volcanic eruptions generally suppress tropical rainfall in the entire tropics resulting from their impact on the global radiation budget and precipitation efficiency (*e.g.*, Spencer *et al.* 1998; Soden *et al.* 2002). The two eruptions hence project a tropical rainfall oscillation within a periodicity band peaking at about 9 years. Therefore, on the interannual-to-interdecadal time scales tropical total rainfall variability is mostly controlled by the volcanic eruptions and factors discussed in Su and Neelin (2004). Also, the tropospheric quasi-biennial oscillation seems to be another important component at the high-frequency end of interannual time scale (Fig. 8; *e.g.*, Rasmusson and Carpenter 1982; Jiang *et al.* 1995; Meehl 1997), and has to be further quantified in the future.

Regarding the long-term rainfall change, globally it tends to approach zero. However, an upward linear trend (0.0584 *mm day^{-1}/decade*) is found over tropical ocean within the 5% confidence level. A downward trend (-0.0192 *mm day^{-1}/decade*) is also found in the rainfall

anomalies over tropical land, though it is not statistically significant (lower than the 20% confidence level). For the tropical total rainfall, the upward trend (0.0373 *mm day^{-1}/decade*) can reach the 10% confidence level. These changes correspond to an about 4.9% rainfall increase over tropical ocean and 1.6% decrease over land during the entire data record.

A linear regression method is applied to the data set to extract the relations of rainfall anomalies with ENSO and volcanoes, respectively, by assuming the impacts of ENSO and volcanoes are separable to a certain extent. After their impacts are assessed, isolated and removed from the rainfall anomalies, the trends for the annual mean rainfall over tropical ocean, land, and the entire tropics are re-examined. The trend for land rainfall is still not statistically significant. However, the linear changes for the tropical total rainfall and oceanic rainfall both reach higher confidence levels, 4% and 1%, respectively, though the magnitudes of the trends become slightly smaller. This is primarily because of a larger *dof* and less variance in the modified data set.

The results here seem to suggest that at least an upward increase in tropical oceanic rainfall is occurring. It tends to support that there is an intensifying hydrological cycle in the tropics given a warming environment (*e.g.,* Yang *et al.* 2003; Neelin *et al.* 2003; Kumar *et al.* 2004). However, with the impact of ENSO and volcano, the linear trends could not reach a relatively comfortable confidence level, for instance, 1%, even for the rainfall changes over the tropical ocean. This is primarily due to the relatively short data record. To reach the 1% confidence level approximately a 43-year and 51-year length of data record would be needed for the tropical oceanic and total rainfall, respectively, if the time-persistence is assumed for any variability on the interannual-to-interdecadal time scales.

15

Acknowledgements

References

Adler, R. F., G. J. Huffman, A. Chang, R. Ferraro, P. Xie, J. Janowiak, B. Rudolf, U. Schneider, S. Curtis, D. Bolvin, A. Gruber, J. Susskind, and P. Arkin, 2003: The version 2 Global Precipitation Climatology Project (GPCP) monthly precipitation analysis (1979-present). *J. Hydrometeor*, **4**, 1147-1167.

Bates, J.J., and D.L. Jackson, 2001: Trends in upper-tropospheric humidity. *Geophys. Res. Lett.,* **28**, 1695-1698.

Bretherton, C.S., M. Widmann, V.P. Dymnikov, J.M. Wallace, and I. Bladé, 1999: The effective number of spatial degree of freedom of a time-varying field. *J. Climate*, **12**, 1990-2009.

Chen, J., B.C. Carlson, and A.D. Del Genio, 2002: Evidence for strengthening of the tropical general circulation in 1990s. *Science*, **295**, 838-841.

Chu, P.-S., and J.-B. Wang, 1997: Recent climate change in the tropical western Pacific and Indian ocean regions as detected by outgoing longwave radiation records. *J. Climate*, **10**, 636-646.

Curtis, S., and R. F. Adler, 2003: The evolution of El Niño-precipitation relationships from satellites and gauges. *J. Geophys. Res.,* **108**(D4), 4153, doi:10.1029/2002JD002690.

Huffman, G. J., and Coauthors, 1997: The Global Precipitation Climatology Project (GPCP) version 1 dataset. *Bull. Amer. Meteor. Soc.,* **78**, 5-20.

Hurrell, J.W., Y. Kushnir, and M. Visbeck, 2001: The North Atlantic Oscillation. *Science,* **291,** 603-605.

Jiang, N., J.D. Neelin, and M. Ghil, 1995: Quasi-quadrennial and quasi-biennial variability in COADS equatorial Pacific sea surface temperature and winds. *Clim. Dyn.,* **12,** 101-112.

Kumar, A., F. Yang, L. Goddard, and S. Schubert, 2004: Differing trends in the tropical surface temperatures and precipitation over land and oceans. *J. Climate,* **17,** 653-664.

Livezey, R.E., and W.Y. Chen, 1983: Statistical field significance and its determination by Monte Carlo techniques. *Mon. Wea. Rev.,* **111,** 46-59.

McCarthy, M.P., and R. Toumi, 2004: Observed interannual variability of tropical troposphere relative humidity. *J. Climate,* **17,** 3181-3191.

Meehl, G.A., 1997: The South Asian monsoon and the tropospheric biennial oscillation. *J. Climate,* **10,** 1921-1943.

Neelin, J.D., C. Chou, and H. Su, 2003: Tropical drought regions in global warming and El Niño teleconnections. *Geophys. Res. Lett.,* **30,** 242275, doi:10.1029/2003GL018625.

Rasmusson, E.M., and T.H. Carpenter, 1982: Variations in tropical sea surface temperature and surface wind fields associated with the Southern Oscillation/El Niño. *Mon. Wea. Rev.,* **110,** 354-384.

Robock, A., 2000: Volcanic eruptions and climate. *Rev. Geophys.,* **38,** 191-219.

Sato, M., J.E. Hansen, M.P. McCormick, and J.B. Pollack, 1993: Stratospheric aerosol optical depths, 1850-1990. *J. Geophys. Res.,* **98,** 22987-22994.

Simmons, A.J., *et al.,* 2004: Comparison of trends and low-frequency variability in CRU, ERA-40, and NCEP/NCAR analyses of surface air temperature. *J. Geophys. Res.,* **109,** D24115, doi:10.1029/2004JD005306.

Soden, B.J., R.T. Wetherald, G.L. Stenchikov, and A. Robock, 2002: Global cooling after the eruption of Mount Pinatubo: A test of climate feedback by water vapor. *Science*, **296**, 727-730.

Spencer, R.W., F.J. LaFontaine, T. DeFelicee, and F.J. Wentz, 1998: Tropical oceanic precipitation changes after the 1991 Pinatubo eruption. *J. Atmos. Sci.*, **55**, 1707-1713.

Su, H., and J.D. Neelin, 2003: The scatter in tropical average precipitation anomalies. *J. Climate*, **16**, 3966-3977.

Sun, D.-Z., T. Zhang, and S.-I. Shin, 2004: The effect of subtropical cooling on the amplitude of ENSO: A numerical study. *J. Climate*, **17**, 3786-3798.

Trenberth, K.E., G.W. Branstator, D. Karoly, A. Kumar, N.-C. Lau, and C. Ropelewski, 1998: Progress during TOGA in understanding and modeling global teleconnections associated with tropical sea surface temperatures. *J. Geophys. Res.*, **103** (C7), 14291-14324.

Trenberth, K.E., J.M. Caron, D.P. Stepaniak, and S. Worley, 2002: Evolution of El Niño-Southern Oscillation and global atmospheric surface temperatures. *J. Geophys. Res.*, **107** (D8), doi:10.1029/2000JD000298.

Vimont, D.J., J.M. Wallace, and D.S. Battisti, 2003: The seasonal footprinting mechanism in the Pacific: Implication for ENSO. *J. Climate*, **16**, 2668-2675.

Wigley, T.M.L., 2000: ENSO, volcanoes and record-breaking temperatures. *Geophys. Res. Lett.*, **27**, 4101-4104.

Woodward, W.A., and H.L. Gray, 1993: Global warming and problem of testing for trend in time series data. *J. Climate*, **6**, 953-962.

Yang, F., A. Kumar, M.E. Schlesinger, and W. Wang, 2003: Intensity of hydrological cycles in warmer climates. *J. Climate*, **16**, 2419-2423.

Yang, F., and M.E. Schlesinger, 2002: On the surface and atmospheric temperature changes following the 1991 Pinatubo volcanic eruption: A GCM study. *J. Geophys. Res.*, **107** (D8), doi:10.1029/2001JD000373.

Yin, X., A. Gruber, and P. Arkin, 2004: Comparison of the GPCP and CMAP merged gauge-satellite monthly precipitation products for the period 1979-2001. *J. Hydrometeor.*, **5**, 1207-1222.

Zhang, Y., J.M. Wallace, and D.S. Battisti, 1997: ENSO-like interdecadal variability: 1900-93. *J Climate*, **10**, 1004-1020.

Table Legends:

Table 1 Mean rainfall and interannual standard deviation (Std) (*mm day^{-1}*) over land and ocean during January 1979-December 2004.

Table 2 Mean rainfall and interannual standard deviation (Std) (*mm day^{-1}*) over ocean during January 1979-December 2004.

Table 3 Mean rainfall and interannual standard deviation (Std) (*mm day^{-1}*) over land during January 1979-December 2004.

Table 4 Linear trends in annual mean rainfall anomalies (*mm day^{-1}/decade*) in the tropics (25°S-25°N) during 1979-2004. The confidence levels are estimated based on the Student's t-test; the degree of freedom (*dof*) are estimated by means of *dof=n(1-γ)/(1+γ)-2, γ* the lag-one correlation coefficient and *n(=26)* the length of time series.

Figure Captions:

Figure 1 Annual mean global rainfall anomalies over ocean, land, and both ocean and land. Also shown are their corresponding linear trends.

Figure 2 Volume contributions to long-time change/linear trend during 1979-2004.

Figure 3 Volume contributions to long-time change/linear trend during 1988-2004.

Figure 4 (a) Tropical mean rainfall anomalies ($mm\ day^{-1}$; 3-month-running-mean); (b) Nino3.4 (^{o}C); and (c) global mean stratospheric aerosol optical thickness (τ_{st}) during 1979-2004.

Figure 5 Annual mean rainfall anomalies over tropical ocean versus land. Dashed line represents the regression between these two during all years except 1982, 1983, 1984, 1991, 1992, and 1993 (dot-crosses) in which an intense volcanic impact is expected (at least 6 months with $\tau_{st} \geq 0.02$).

Figure 6 Tropical rainfall anomalies ($mm\ day^{-1}$; 3-month-running-mean) as function of Nino3.4 (^{o}C) over (a) ocean, (b) land, and (c) both ocean and land. Dots (crosses) denote the months in which $\tau_{st} < (\geq)\ 0.02$, with solid (dashed) lines representing their corresponding linear fit lines.

Figure 7 Tropical rainfall anomalies ($mm\ day^{-1}$; 3-month-running-mean) as function of τ_{st} during the intense volcanic impact period (a) with and (b) without the ENSO impact. Dots denote the tropical total rainfall anomalies, crosses the anomalies over land, and diamonds the anomalies over ocean. Their corresponding linear fits are represented by solid (dots), dashdot (diamonds), and dashed (crosses) lines.

Figure 8 Tropical mean rainfall anomalies ($mm\ day^{-1}$) band-pass-filtered between 2-7 years (a) with, (b) without the ENSO impact, and (c) without the impact from either ENSO or volcano.

Figure 9 Spectral power of tropical total and oceanic rainfall anomalies (($mm\ day^{-1}$) with and without the impact of ENSO and volcano.

Figure 10 Annual mean tropical rainfall anomalies (a) with and (b) without the ENSO and volcano impact (see text). Also shown are their corresponding linear trends.

Table 1 Mean rainfall and interannual standard deviation (Std) ($mm\ day^{-1}$) over land and ocean during January 1979-December 2004.

	Globe	25°S-25°N	25°S-50°S	50°S-90°S	25°N-50°N	50°N-90°N
Mean	2.61	3.11	2.60	2.07	2.35	1.76
Std	0.06	0.12	0.26	0.27	0.20	0.33

Table 2 Mean rainfall and interannual standard deviation (Std) ($mm\ day^{-1}$) over ocean during January 1979-December 2004.

	Globe	25°S-25°N	25°S-50°S	50°S-90°S	25°N-50°N	50°N-90°N
Mean	2.85	3.08	2.70	2.49	3.12	2.04
Std	0.10	0.17	0.30	0.33	0.54	0.47

Table 3 Mean rainfall and interannual standard deviation (Std) ($mm\ day^{-1}$) over land during January 1979-December 2004.

	Globe	25°S-25°N	25°S-50°S	50°S-90°S	25°N-50°N	50°N-90°N
Mean	2.09	3.19	1.86	0.67	1.54	1.56
Std	0.15	0.29	0.40	0.15	0.33	0.36

Table 4 Linear trends in annual mean rainfall anomalies ($mm\ day^{-1}/decade$) in the tropics (25°S-25°N) during 1979-2004. The confidence levels are estimated based on the Student's t-test; the degrees of freedom (dof) are estimated by means of $dof=n(1-\gamma)/(1+\gamma)-2$, γ the lag-one correlation coefficient and $n(=26)$ the length of time series.

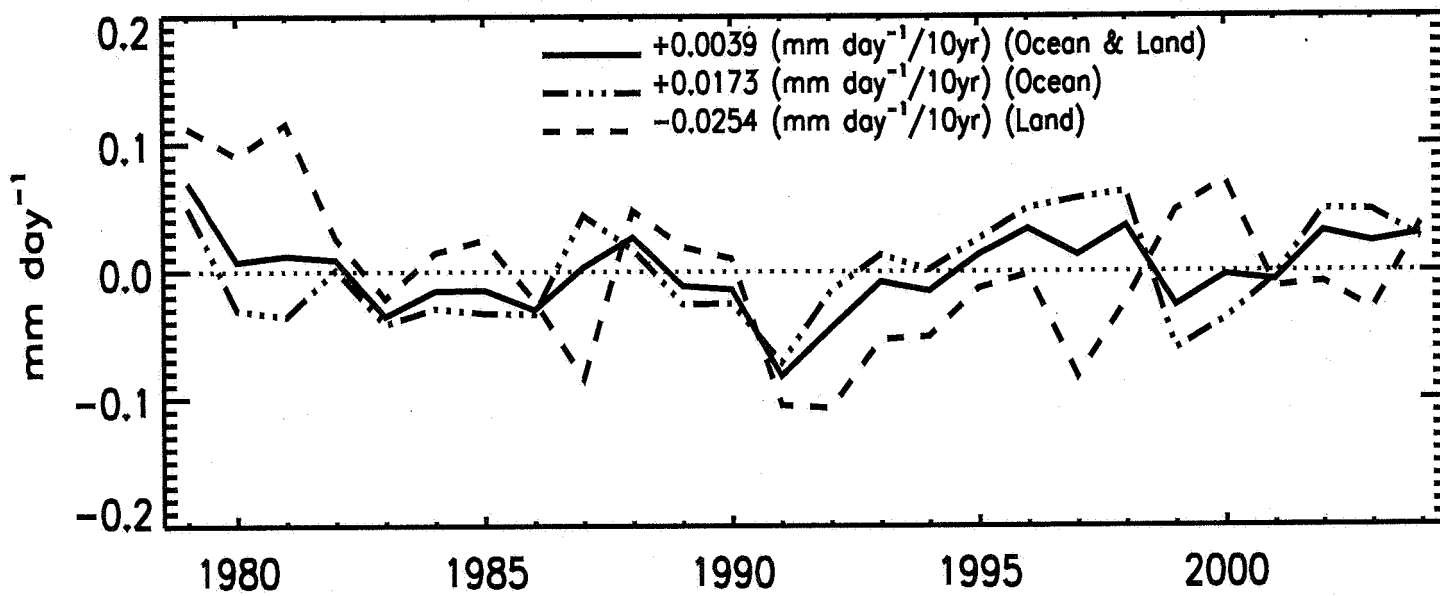|	Trend (Confidence Level)			
	Original		Without ENSO or Volcanoes	
Land & Ocean	0.0373 (10%)	*dof=10*	0.0323 (4%)	*Dof=14*
Land	-0.0192 (<20%)	*dof=11*	-0.0311 (<20%)	*Dof=12*
Ocean	0.0584 (5%)	*dof=10*	0.0559(1%)	*Dof=14*

Figure 1: Annual mean global rainfall anomalies over ocean, land, and both ocean and land. Also shown are their corresponding linear trends.
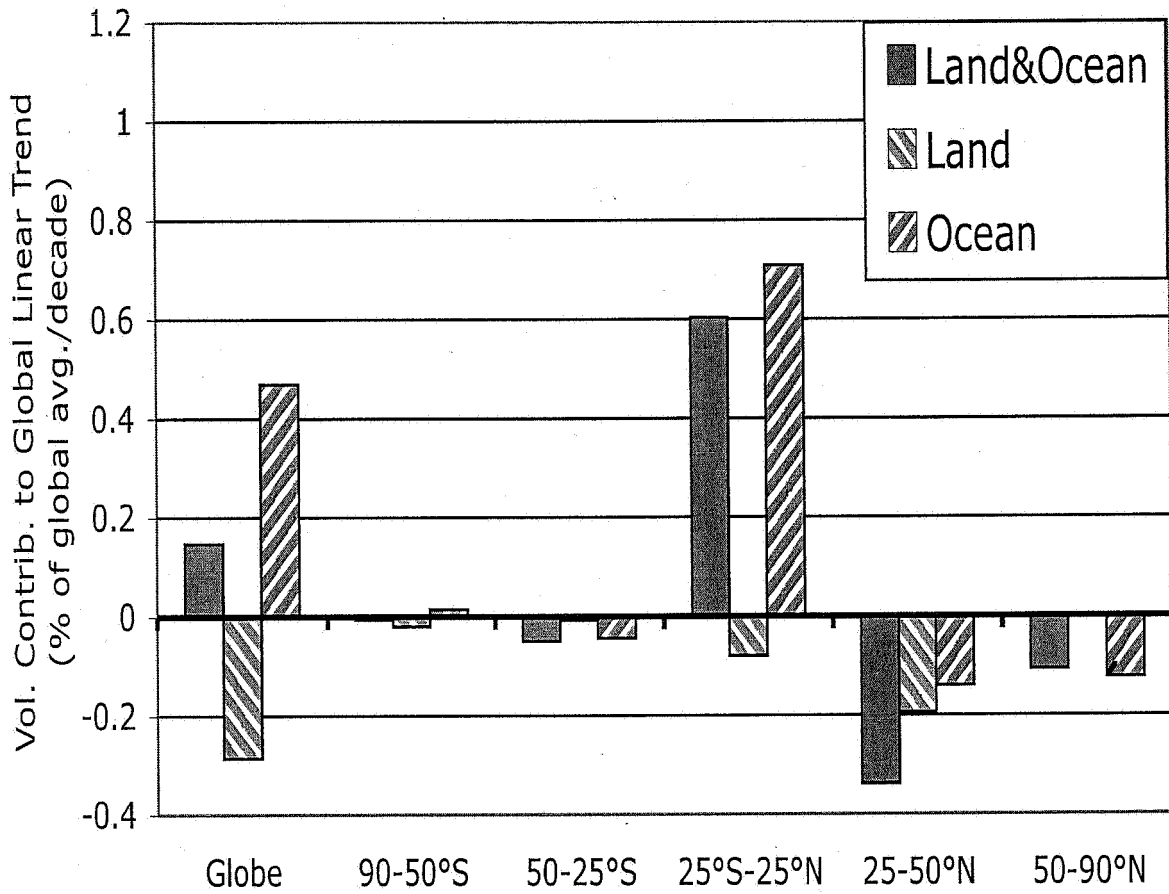
GPCP V.2 1979-2004

Figure 2: Volume contributions to long-time change/linear trend during 1979-2004.
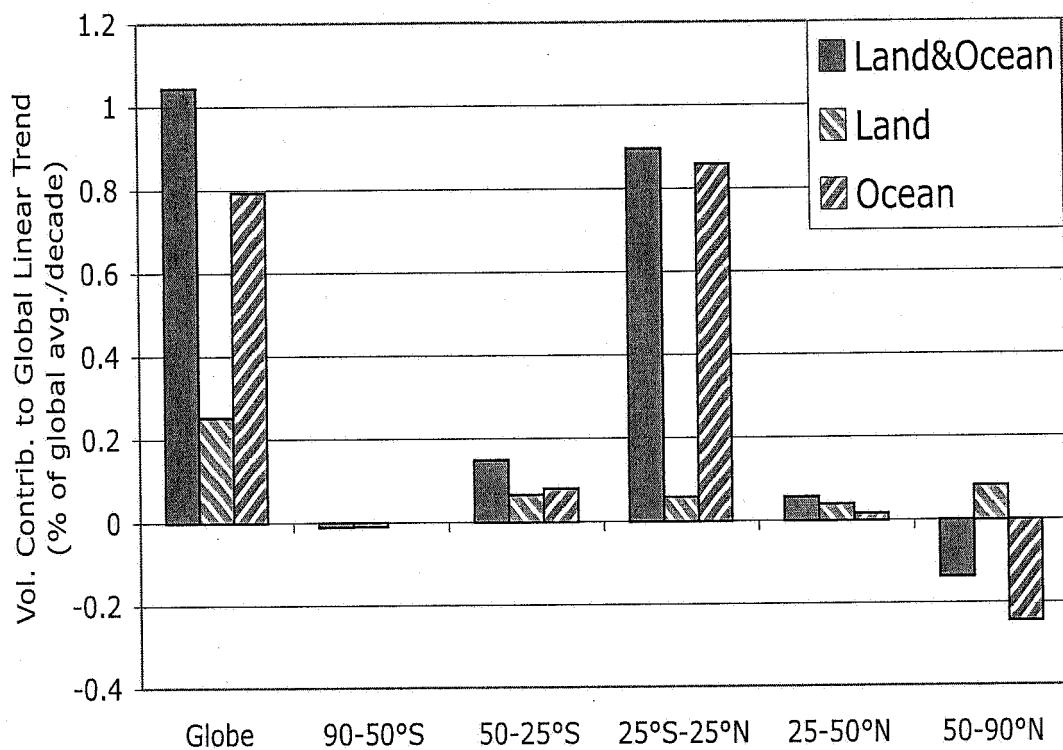
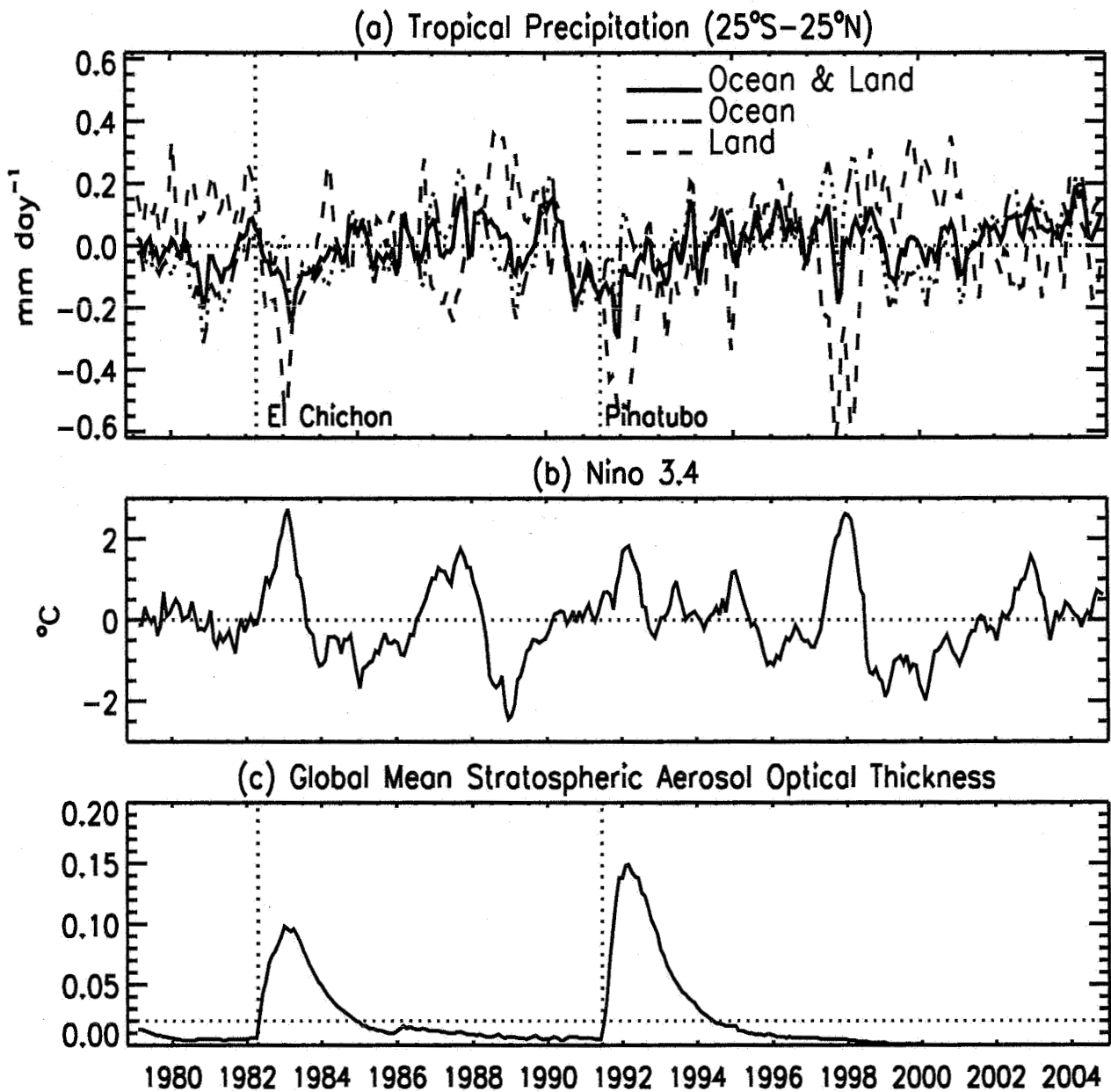Figure 3: Volume contributions to long-time change/linear trend during 1988-2004.

Figure 4: (a) Tropical mean rainfall anomalies ($mm\ day^{-1}$; 3-month-running-mean); (b) Nino 3.4 (^oC); and (c) global mean stratospheric aerosol optical thickness (τ_{st}) during 1979-1999.
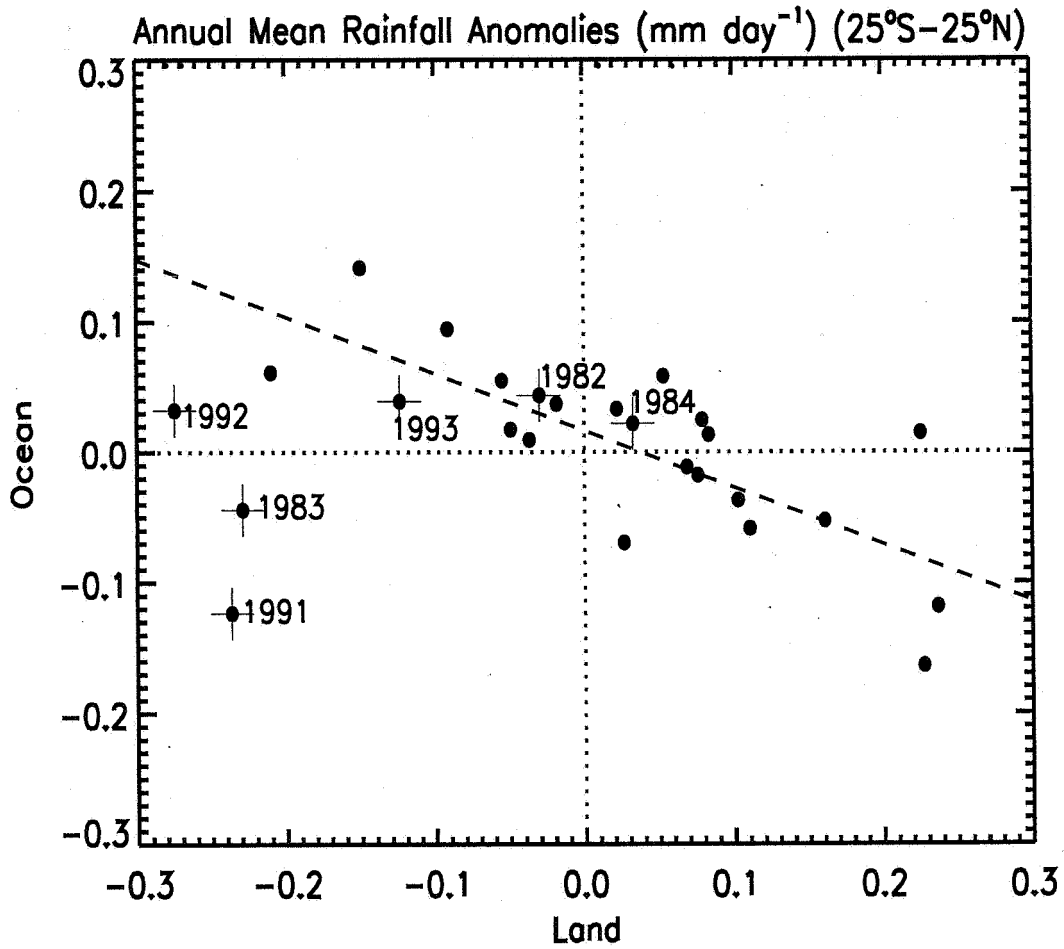
Figure 5: Annual mean rainfall anomalies over tropical oceans vs lands. Dashed line represents the regression between these two during all years except 1982, 1983, 1984, 1991, 1992 and 1993 (dot-crosses) in which an intense volcanic impact is expected (at least 6 months with the global mean stratospheric aerosol optical thickness $\tau_{st} \geq 0.02$).
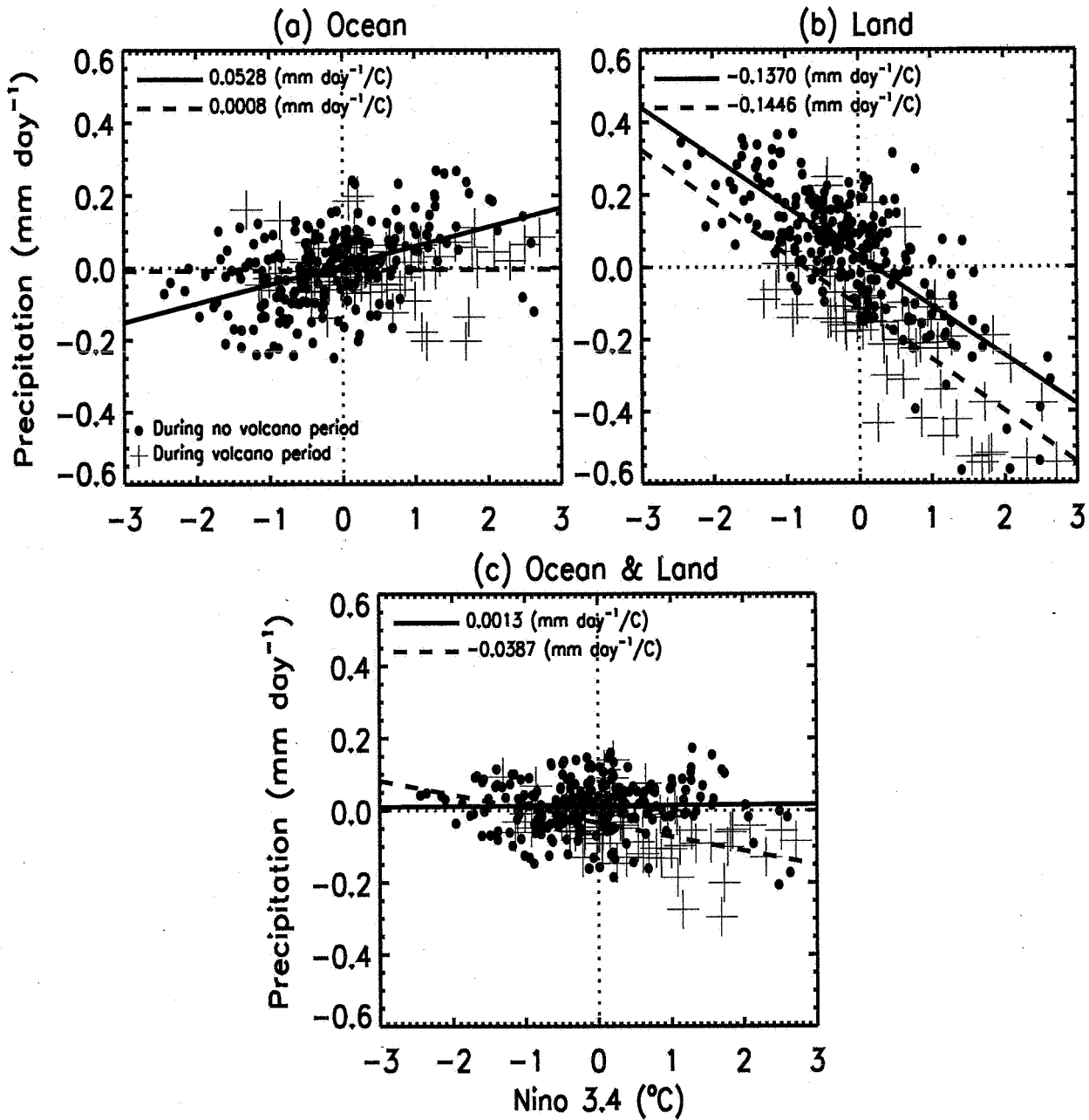
Figure 6: Tropical rainfall anomalies ($mm\ day^{-1}$; 3-month-running-mean) as function of Nino 3.4 (^{o}C). (a) Over ocean, (b) over land, and (c) over both ocean and land. Dots (crosses) denote the months in which the global mean stratospheric aerosol optical thickness $\tau_{st} < (\geq)\ 0.02$, with solid (dashed) lines representing their corresponding linear fit lines.
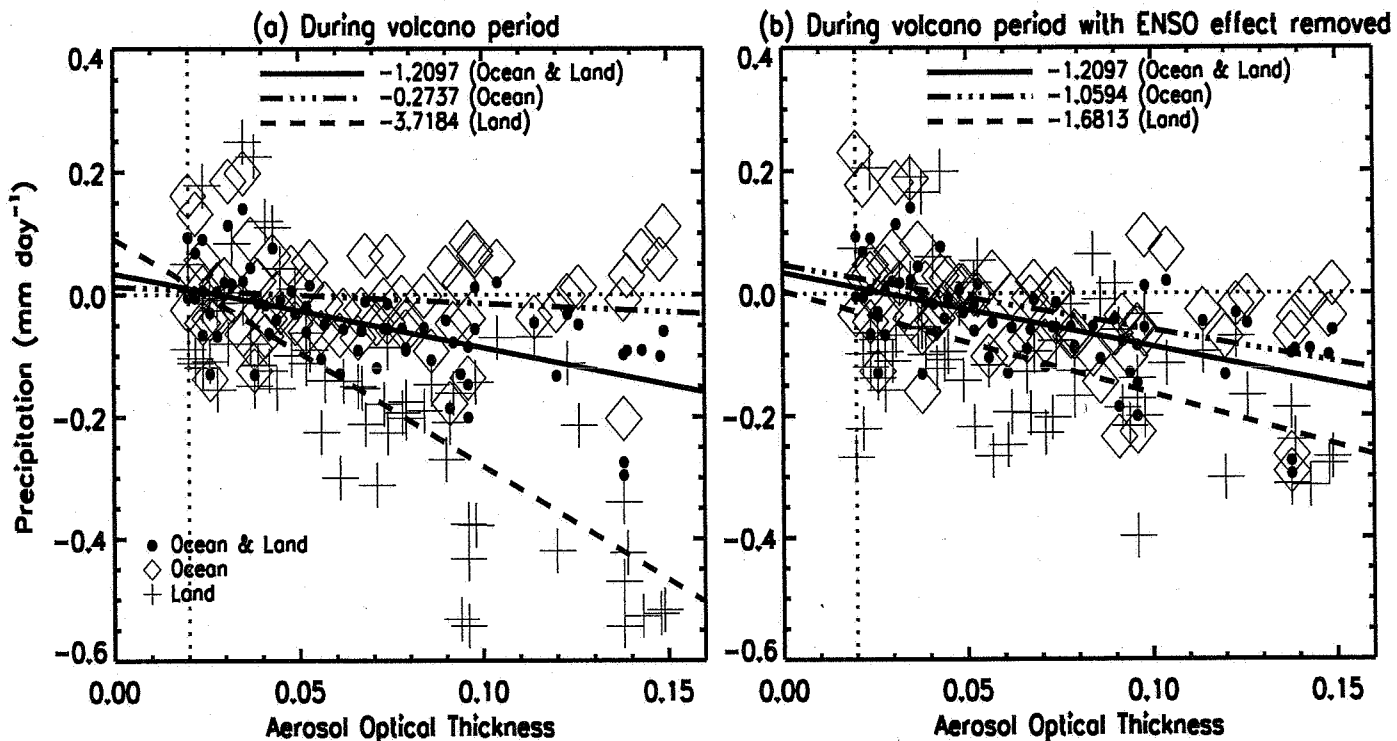
Figure 7: Tropical rainfall anomalies ($mm\ day^{-1}$; 3-month-running-mean) as function of the magnitude of the global mean stratospheric aerosol optical thickness (τ_{st}) during the intense volcanic impact period (a) with and (b) without the impact of ENSO. Dots denote the total tropical rainfall anomalies, crosses the anomalies over land, and diamonds the anomalies over ocean. Their corresponding linear fits are represented by solid (dots), dashdot (diamonds), and dashed (crosses) lines.
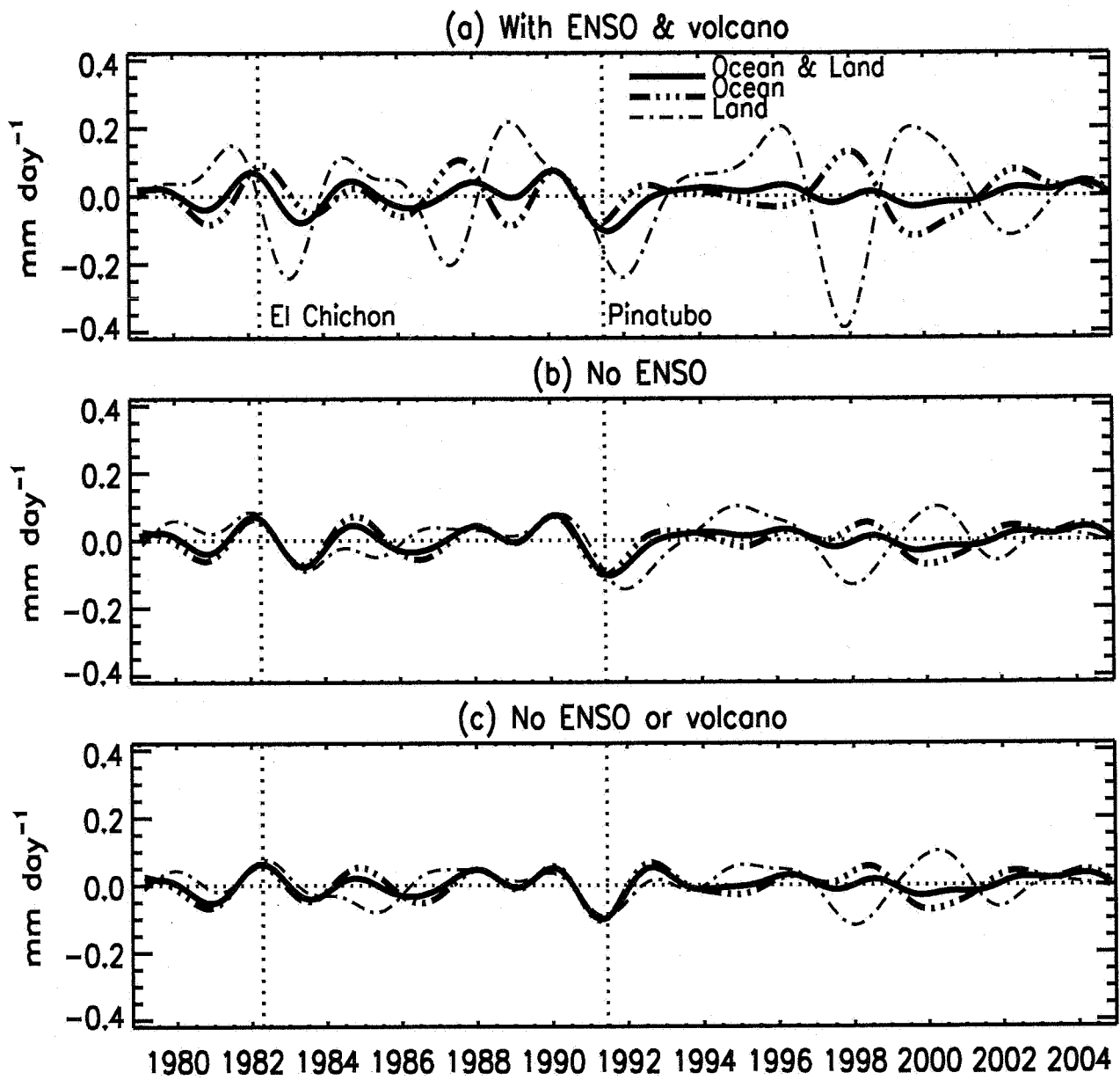
Figure 8: Tropical mean rainfall anomalies ($mm\ day^{-1}$) band-pass-filtered between 2-7 years (a) with, (b) without the impact of ENSO, and (c) without the impact from either ENSO or volcane (see text).
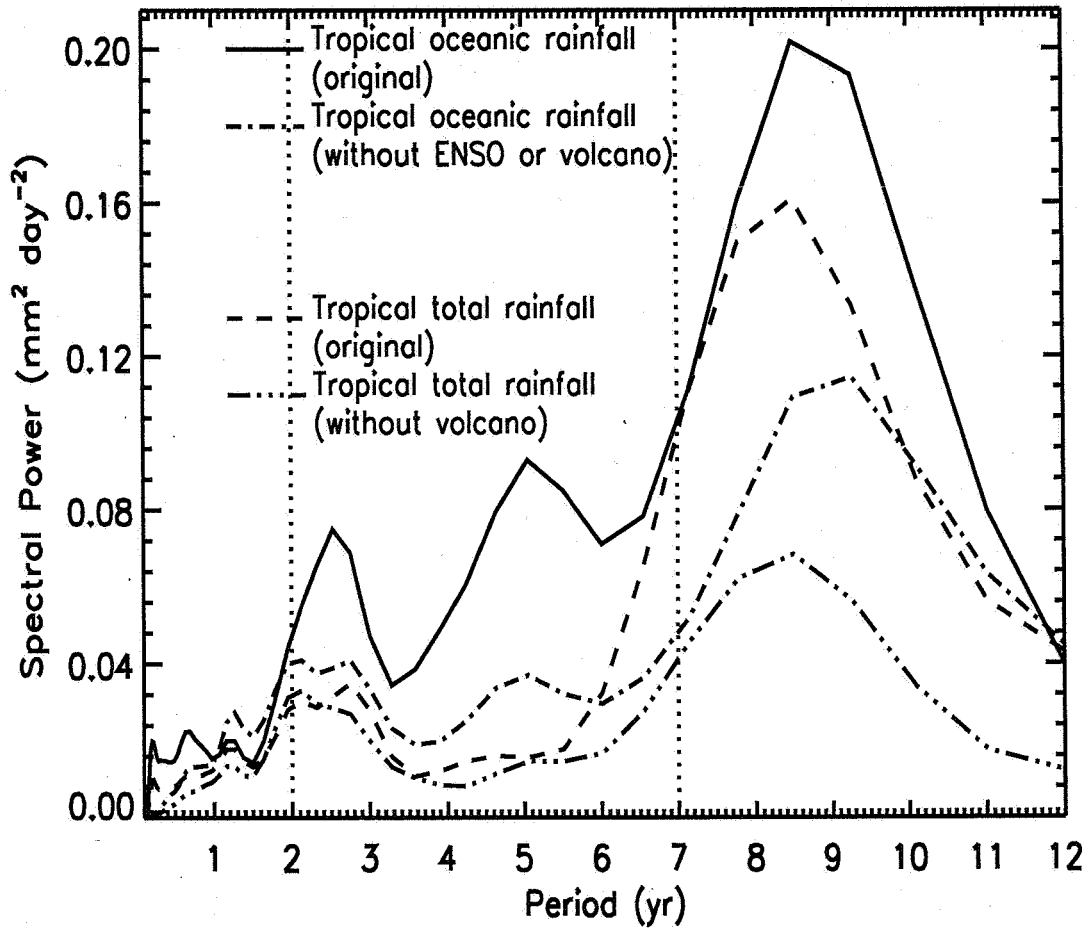
27

Figure 9: Spectral power of tropical total and oceanic rainfall anomalies ($mm\ day^{-1}$) with and without the impact of ENSO and volcano.
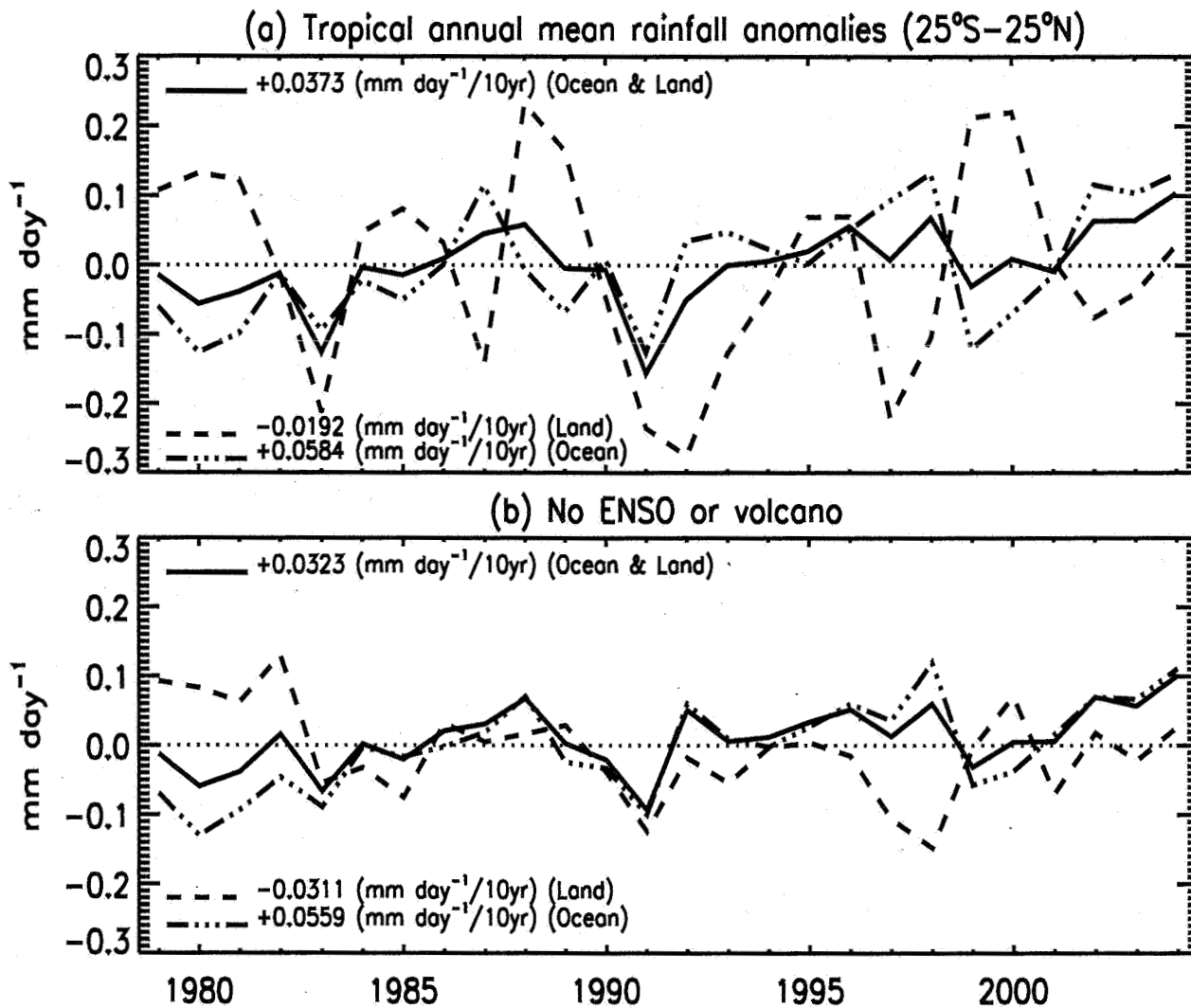
Figure 10: Annual mean tropical rainfall anomalies (a) with and (b) without the ENSO and volcanic impact which is removed by means of a regression method (see text). Also shown are their corresponding linear trends.